THE JOURNAL OF PHYSICAL CHEMISTRY C

Article

pubs.acs.org/JPCC

Electronic Stability of Phosphine-Protected Au_{20} Nanocluster: Superatomic Bonding

Yuan Yuan,[†] Longjiu Cheng,*[,†] and Jinlong Yang*[,‡]

[†]Department of Chemistry, Anhui University, Hefei, Anhui, 230039, People's Republic of China

[‡]Hefei National Laboratory for Physics Sciences at the Microscale, University of Science & Technology of China, Hefei, Anhui, 230026, People's Republic of China

Supporting Information

ABSTRACT: A recent experiment reported that a newly crystallized phosphine-protected Au_{20} nanocluster $[Au_{20}(PPhy_2)_{10}Cl_4]Cl_2$ [$PPhpy_2$ = bis(2-pyridyl)phenylphosphine] owns a very stable Au_{20} core, but the number of valence electrons of the Au_{20} core is 14e, which is not predicted by the superatom model. So we apply the density functional theory to further study this cluster from its molecular orbital and chemical bonding. The results suggest that the $Au_{20}^{(+6)}$ core is an analogue of the F_2 molecule based on the super valence bond model, and the 20-center−14-electron $Au_{20}^{(+6)}$ core can be taken as a superatomic molecule bonded by two 11-center−7-electron superatoms, where the two 11c superatoms share two Au atoms and two electrons to meet an 8-electron closed shell for each. The electronic shell closure enhances the stability of the Au_{20} core, besides the PN bridges. Exceptionally, the theoretical HOMO−LUMO gap (1.03 eV) disagrees with the experimental value (2.24 eV), and some possible reasons for this big difference are analyzed in this paper.

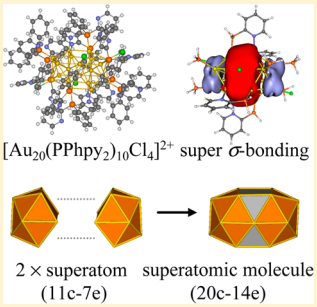

1. INTRODUCTION

Ligand-protected gold nanoclusters have been widely studied due to their interesting optical, electronic, and charging properties, as well as potential applications in catalysis, biomedicine, and nanoelectronics.[1−5] So far, tremendous advances have been achieved in the synthesis and isolation of thiolate-protected Au nanoparticles (RS−AuNPs).[6−15] Among RS-AuNPs, $Au_{25}(SR)_{18}$,[16−29] $Au_{38}(SR)_{24}$,[10,30−38] $Au_{40}(SR)_{24}$,[36,39,40] $Au_{102}(SR)_{44}$,[41−45] and $Au_{144}(SR)_{60}$[46−48] are more extensively studied. Especially, the crystallization and structural determination of Au_{25},[49,50] Au_{36},[51] Au_{38},[35] and Au_{102}[52] were breakthroughs in RS−AuNPs research. Theoretical and experimental studies confirm that $Au_{25}(SR)_{18}^-$ combines an icosahedral Au_{13} core and six dimeric (−RS−Au−RS−Au−RS−) staple motifs.[19,49,50] Similarly, $Au_{38}(SR)_{24}$ is also verified to be composed of a face-fused bi-icosahedral Au_{23} core and six dimeric and three monomeric (−RS−Au−RS−) staple motifs,[35,53,54] and the bi-icosahedral Au_{23} core is proved to be a superatomic molecule consisting of two Au_{13} superatoms.[38] In addition, the gold−phosphane clusters are one of few examples of ligand-protected gold clusters whose structures have been characterized, including some small clusters, Au_{4-10},[55−59] Au_{11},[45,60] and Au_{13},[45,61,62] and large ones, $[Au_{24}(PPh_3)_{10}(SC_2H_4Ph)_5X_2]^+$,[63] $[Au_{39}(PPh_3)_{14}Cl_6]Cl_2$,[64] and $Au_{55}(PPh_3)_2Cl_6$.[65−68]

Recently, Wan et al.[69] isolated a new phosphine-protected Au_{20} nanocluster through the reduction of $Au(PPhpy_2)Cl$ [$PPhpy_2$ = bis(2-pyridyl)phenylphosphine] by $NaBH_4$ and determined its structure by single crystal X-ray structural analysis. This new cluster consists of a dicationic cluster $[Au_{20}(PPhpy_2)_{10}Cl_4]^{2+}$ (**A1**) and two Cl^-, and the dicationic cluster includes one Au_{20} core, ten phosphines ($PPhpy_2$), and four Cl^- ligands. Interestingly, the Au_{20} core can be viewed as the fusion of two Au_{11} incomplete icosahedra by sharing two vertices. Unexpectedly, the HOMO−LUMO gap from the optical absorption spectrum of $[Au_{20}(PPhpy_2)_{10}Cl_4]Cl_2$ is high, 2.24 eV, which arouses our curiosity (the magic stable $Au_{25}(SR)_{18}^-$, $E_{HOMO-LUMO}$ = 1.30 eV;[50,51,70] $Au_{38}(SR)_{24}$, $E_{HOMO-LUMO}$ = 0.90 eV).[51,71,72] Besides, the $[Au_{20}(PPhpy_2)_{10}Cl_4]^{2+}$ cluster with 14 (n = 20 − 4 − 2) valence electrons is not a closed shell, and they suggest that the stability of the $Au_{20}^{(+6)}$ core benefits from only geometric symmetry, and the nanocluster is stabilized by the PN bridges. However, we think that the electronic structure of this nanocluster may be interesting and the electronic factors should also make some contribution to the stability of the nanocluster. As to these doubts above, we perform a computational study based on density functional theory (DFT) calculation to analyze this new phosphine-protected Au_{20} nanocluster.

2. COMPUTATIONAL METHODS

The atomic coordinates (see the Supporting Information) of newly crystallized cluster $[Au_{20}(PPhpy_2)_{10}Cl_4]Cl_2$ are obtained from its single-crystal structure. The Perdew−Burke−Ernzerhof (PBE) functional[73] is selected in DFT, which was proven to give the results in good agreement with experimental data in ligand-protected Au nanoclusters.[5,32,40,42,67,68,74,75] Due to

Received: March 21, 2013
Revised: May 9, 2013
Published: June 3, 2013

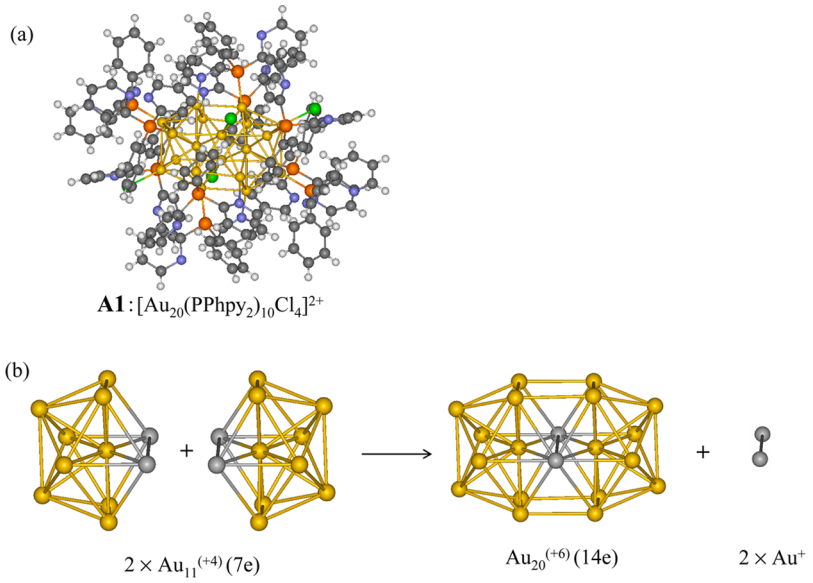

Figure 1. (a) The structure of dicationic $[Au_{20}(PPhpy_2)_{10}Cl_4]^{2+}$ (**A1**) cluster (Au, yellow; P, orange-brown; N, blue; C, dark gray; H, white; Cl, green). (b) Superatomic model for $Au_{20}^{(+6)}$ core.

computational difficulty, we replaced the Ph and partial py (except for the py of four PN bridges, py = pyridyl) with H in our calculations. The initial geometry of $[Au_{20}(PH_3)_6(PH_2py)_4Cl_4]^{2+}$ (**A2**; see the Supporting Information) was relaxed at the PBE/6-31G* and lanl2dz levels. The calculations of MO and chemical bonding analyses were performed by the PBE functional (F, H, C, N, P, Cl at the 3-21G level and Au at the lanl2dz level). The UV−vis absorption spectra of **A2** is simulated at the PBE/6-31G*/lanl2dz level. The HOMO−LUMO gap of **A1** is also calculated at the PBE/6-31G*/lanl2dz level. All calculations are carried out using the Gaussian 09 package.[76]

3. RESULTS AND DISCUSSION

The geometric structure of **A1** is shown in Figure 1a. On the basis of the analyses of Wan et al., we suggest that the Au_{20} core (Figure 1b) is made up of two 11 center−7 electron (11c−7e) incomplete icosahedral units by sharing two vertices and owns 14 valence electrons. Here the number of valence electrons of the Au_{20} core is identical to that of one F_2 molecule. Then, in the electronic structure, is the $Au_{20}^{(+6)}$ core also similar to that of the F_2 molecule? In order to confirm this supposition, we first make a comparison of the canonical Kohn−Sham molecular orbitals (MOs) of valence shell between $Au_{20}^{(+6)}$ and the F_2 molecule, and the results are displayed in Figure 2. According to valence bond theory, F_2 molecule has three lone pairs in each F atom and one covalent pair shared by two F atoms. The electronic configuration of the F_2 molecule is $(\sigma_s)^2(\sigma^*_s)^2(\sigma_{p_z})^2(\pi_{p_xp_y})^4(\pi^*_{p_xp_y})^4(\sigma^*_{p_z})^0$. Among these, the π_{p_x} ($\pi^*_{p_x}$) and π_{p_y} ($\pi^*_{p_y}$) are doubly degenerate, the $(\sigma_{p_z})^2$ MO constitutes the F−F σ-bond, and the energy gap of $\pi^*_{p_xp_y}$ and $\sigma^*_{p_z}$ is the HOMO−LUMO gap. In the canonical MOs of $Au_{20}^{(+6)}$, the π_{p_x} ($\pi^*_{p_x}$) and π_{p_y} ($\pi^*_{p_y}$) should also be doubly degenerate as well as those of F_2, but the degenerate orbitals are in different energy levels because of their geometric symmetry. The d_{xy} atomic orbital is split into $\delta_{d_{xy}}$ and $\delta^*_{d_{xy}}$ and the $d_{x^2-y^2}$ is split into $\delta_{d_{x2-y2}}$ and $\delta^*_{d_{x2-y2}}$ ($\delta^*_{d_{xy}}$ and $\delta^*_{d_{x2-y2}}$ are not plotted in this figure). The $\delta_{d_{xy}}$ and $\delta_{d_{x2-y2}}$ should also be doubly degenerate, which are lower than $\sigma^*_{p_z}$ in energy. The electronic configuration of $Au_{20}^{(+6)}$ in this example is $(\sigma_s)^2(\sigma^*_s)^2(\pi_{p_x})^2(\pi_{p_y})^2(\pi^*_{p_y})^2(\sigma_{p_z})^2(\pi^*_{p_x})^2(\delta_{d_{xy}})^0(\delta_{d_{x2-y2}})^0(\sigma^*_{p_z})^0$. Its HOMO−LUMO gap is the energy difference between $\pi^*_{p_x}$ and $\delta_{d_{xy}}$. On the whole, the canonical MOs of $Au_{20}^{(+6)}$ are similar to those of F_2 in shape and energy sequence, and only the energy sequence of σ_{p_z}, π_{p_x}, and π_{p_y} is different. Therefore, $Au_{20}^{(+6)}$ is exactly analogous of F_2 molecule, which can be viewed as a superatomic molecule bonded by two 11c−7e superatoms. And each superatom satisfies the 8-electron shell

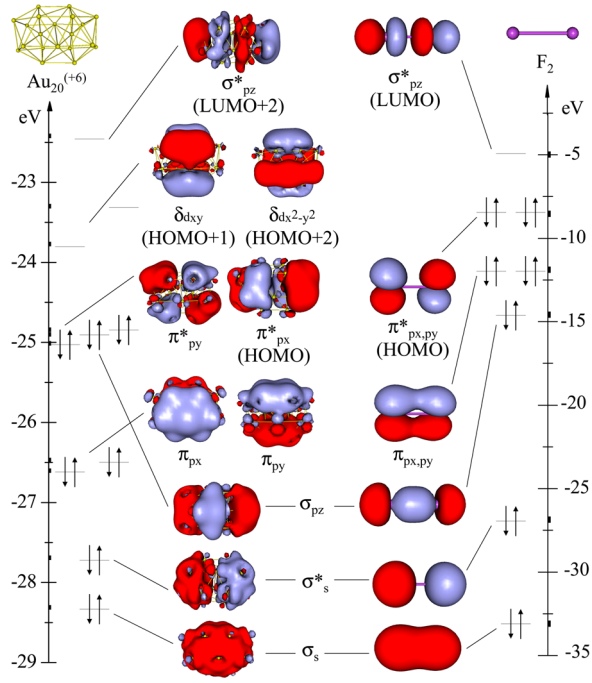

Figure 2. Comparison of the Kohn−Sham MO diagrams between $Au_{20}^{(+6)}$ (left) and F_2 (right).

dx.doi.org/10.1021/jp402816b | J. Phys. Chem. C 2013, 117, 13276−13282

closure by sharing two electrons, like the F atom of F_2, which can account for the stability of $Au_{20}^{(+6)}$ cluster.

In addition, the Au_{23} core of the $Au_{38}(SR)_{24}$ cluster was also reported to be an analogue of F_2 molecule.[38] However, the MO energy-level order of $Au_{20}^{(+6)}$ cluster is different from that of the Au_{23} core of $Au_{38}(SR)_{24}$ cluster $[(\sigma_s)^2(\sigma^*_s)^2(\pi_{p_x p_y})^4(\sigma_{p_z})^2(\pi^*_{p_x p_y})^4(\sigma^*_{p_z})^0]$. Here, Figure 3 depicts a schematic representation of the MO energy-level diagram for $Au_{20}^{(+6)}$ superatomic molecule. The π- and δ-type MO energy levels of $Au_{20}^{(+6)}$ are lower. Because the Au_{23} core of $Au_{38}(SR)_{24}$ cluster is a union of two complete icosahedral units, but the Au_{20} core of this nanocluster is bonded by two incomplete icosahedral Au_{11} units, the distance of the two Au_{11} superatoms is closer, which makes the π- and δ-type MO energy level lower.

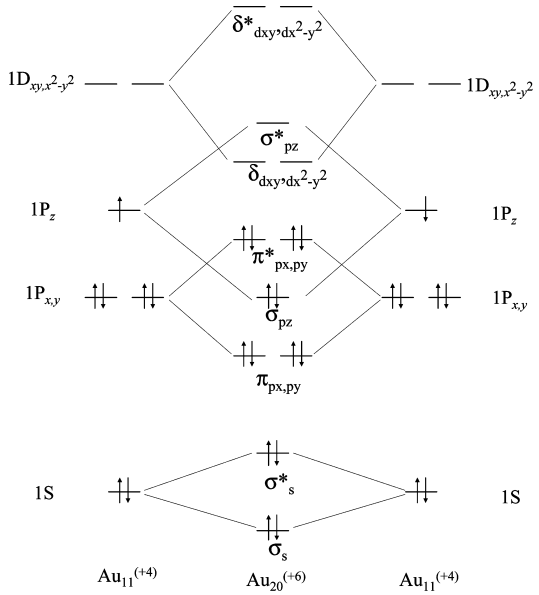

Figure 3. Schematic representation of the MO energy-level diagram for $Au_{20}^{(+6)}$ superatomic molecule.

To further verify the superatomic molecule model of $Au_{20}^{(+6)}$, we apply a new tool named adaptive natural density partitioning (AdNDP) to analyze chemical bonding. This method was recently developed by Zubarev and Boldyrev[77−79] and has been successfully applied to the analysis of chemical bonding in organic aromatic cyclic molecules,[79] boron clusters,[80−82] Au nanoclusters,[38,83] etc. AdNDP is based on the concept of the electron pair as the main element of chemical bonding models, which recovers both Lewis bonding elements (1c−2e and 2c−2e objects) and delocalized bonding elements (nc−2e). The results of AdNDP analysis are shown in Figure 4. On the basis of the concept of super valence bond (SVB)[84] newly proposed by our group, $Au_{20}^{(+6)}$ cluster has three 11c−2e super-lone-pairs (LPs) in each 11c superatom and one 20c−2e super-σ-bond with occupation number (ON) = 2.00 |e| in the whole cluster, where three super-LPs may be viewed as super S, P_x, and P_y, respectively, as shown in Figure 4. According to the above analyses, $Au_{20}^{(+6)}$ cluster indeed can be taken as a superatomic molecule bonded by two 11c−7e superatoms, where the two 11c superatoms share two Au atoms and two electrons.

Generally, the ligand effect plays an important role in ligand-protected Au nanocluster. Therefore, the chemical bonding of the overall cluster $[Au_{20}(PPhpy_2)_{10}Cl_4]^{2+}$ is analyzed by AdNDP. But for simplicity and clarity in analyzing chemical bonding, we use H instead of all Ph and partial py (except for the py of four PN bridges), which is often adopted in Au−SR[5,38] and gold−phosphane−halide clusters.[67,85] The bonding framework of the valence shells of $[Au_{20}(PH_3)_6(PH_2py)_4Cl_4]^{2+}$ (**A2**) using AdNDP is shown in Figure 5. According to the results of AdNDP analysis, there are 88 2c−2e localized σ-bonds with ON = 1.88−1.99 |e| (P−H, P−C, C−N, etc. σ-bonds) and 12 6c−2e delocalized π-bonds of pyridyl with ON = 1.98−2.00 |e| (Figure 5d). In addition, 14 electrons are delocalized in the $Au_{20}^{(+6)}$ core including two s-type, four p-type 11c−2e super-LPs (Figure 5c), and 1 20c−2e super-σ-bond (Figure 5b). The above bonding analysis verifies that the $Au_{20}^{(+6)}$ core of **A1** is a superatomic molecule in electronic structure indeed.

Note that the HOMO−LUMO gap of Au nanocluster mainly depends on the electronic structure of the Au core. Based on the SVB model, the $Au_{20}^{(+6)}$ core can be taken as an analogue of F_2 molecule in chemical bonding, so the HOMO−LUMO gap of **A1** should be approximate to that of $Au_{38}(SR)_{24}$ cluster and lower than that of $Au_{25}(SR)_{18}^-$ cluster [$Au_{38}(SR)_{24}$, $E_{HOMO-LUMO}$ = 0.90 eV; the $Au_{23}^{(+9)}$ core of $Au_{38}(SR)_{24}$ cluster is verified to be also an analogue of F_2 molecule; $Au_{25}(SR)_{18}^-$, $E_{HOMO-LUMO}$ = 1.30 eV; $Au_{25}(SR)_{18}^-$ can be seen as a super-Ne

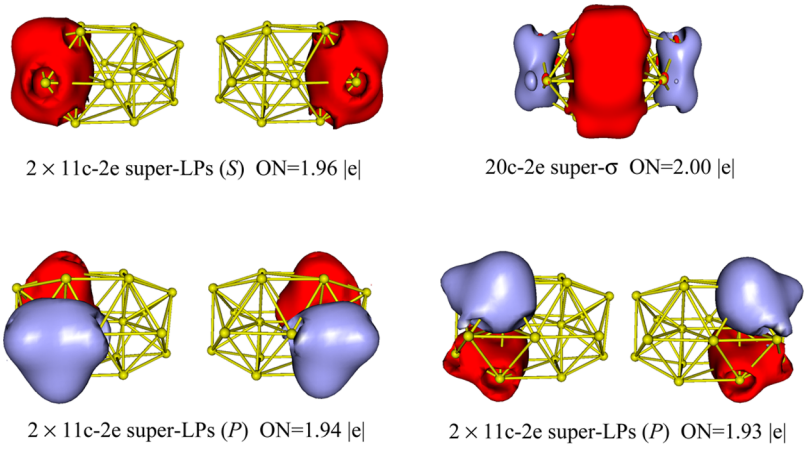

Figure 4. AdNDP localized natural bonding orbitals of $Au_{20}^{(+6)}$ cluster.

dx.doi.org/10.1021/jp402816b | J. Phys. Chem. C 2013, 117, 13276−13282

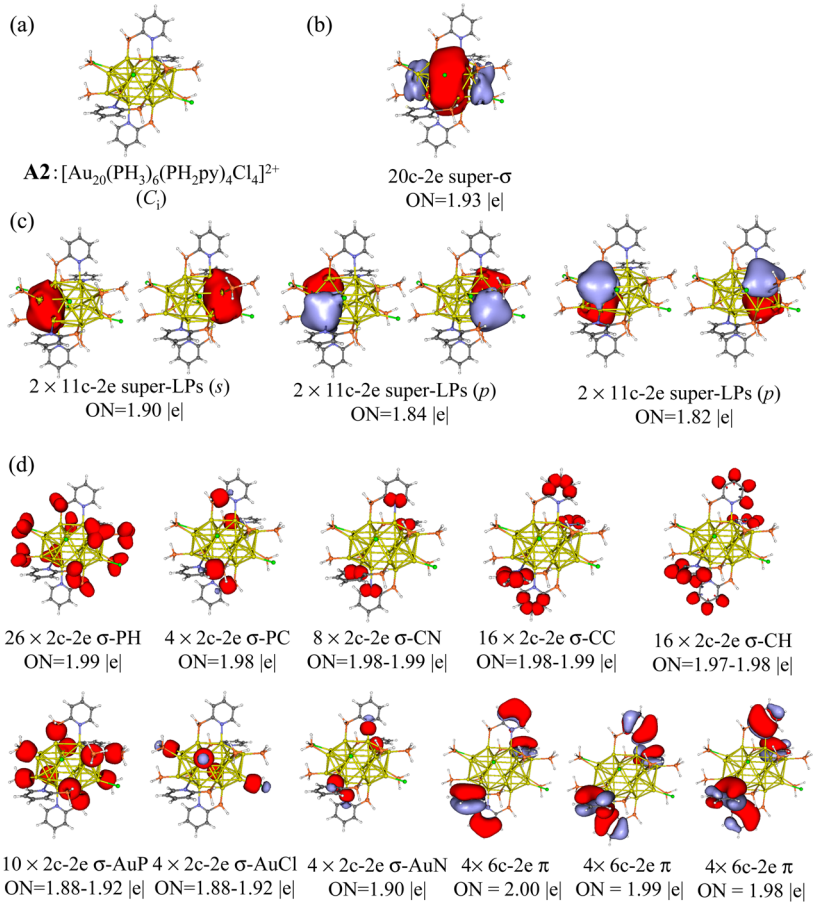

Figure 5. (a) Geometry and AdNDP localized natural bonding orbitals of **A2**: (b) 20c−2e delocalized bonding, (c) 11c−2e delocalized bonding, and (d) 2c−2e localized σ-bonds and 6c−2e delocalized π-bonds.

molecule).[38] However, the experimental HOMO−LUMO gap of **A1** is high, 2.24 eV, which is not in agreement with the theoretical value (**A1**, $E_{HOMO-LUMO}$ = 1.03 eV). To make up for the credibility of our theoretical result, we calculate the HOMO−LUMO gaps of some known Au nanoclusters at the PBE/6-31G*/lanl2dz level, compared with the experimental values, and the results are shown in Table 1. For Au_{20} cluster,

Table 1. The HOMO−LUMO Gaps (in eV) of Au Nanoclusters (R = CH_2CH_2Ph) Calculated at the PBE/6-31G*/lanl2dz Level, Compared with the Experimental Values

clusters	theoretical	experimental
Au_{20} (T_d)	1.89	1.77 (ref 86)
$Au_{25}(SR)_{18}^-$	1.41	1.30 (refs 50, 70)
$Au_{38}(SR)_{24}$	1.01	0.90 (refs 71, 72)
$[Au_{20}(PPhpy_2)Cl_4]^{2+}$	1.03	2.24 (ref 69)

the theoretical gap (1.89 eV) is higher than the experimental value (1.77 eV)[86] by only 0.12 eV. For $Au_{25}(SR)_{18}^-$ and $Au_{38}(SR)_{24}$ clusters, the theoretical gap is also slightly higher than the experimental one (0.11 eV), respectively. So we can see that the HOMO−LUMO gap calculated by the PBE functional is very close to (slightly larger than) the experimental one. Therefore, the PBE functional usually can provide a reliable HOMO−LUMO gap for Au nanoclusters.

However, why is the theoretical HOMO−LUMO gap of **A1** inconsistent with the experimental one? In order to analyze the reasons for this big difference, the ultraviolet−visible (UV−vis) absorption spectra should be simulated to compare with the experimental optical absorption spectra. But because the system of **A1** is so big, it is difficult for us to complete the calculation of UV−vis absorption spectra. So we compute the UV−vis absorption spectra of **A2** instead of **A1**, as shown in Figure 6a. The optical band edge of calculated UV−vis absorption spectra of **A2** is 1.19 eV, which is consistent with the computed

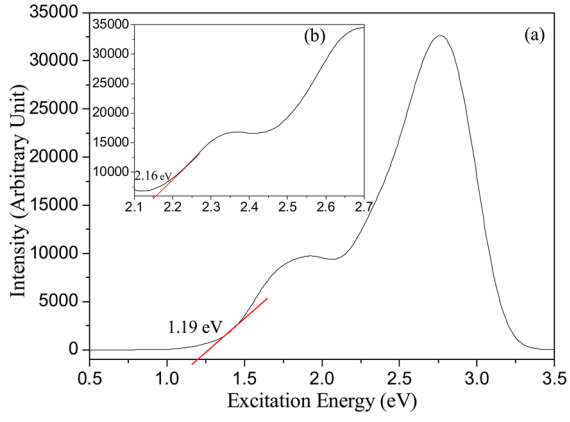

Figure 6. (a) Simulated UV−vis absorption spectra of **A2** at the PBE/6-31G* and lanl2dz level; the HOMO−LUMO gap is 1.19 eV. (b) Enlarged simulated UV−vis absorption spectra of **A2** in the 2.1−2.7 eV region.

dx.doi.org/10.1021/jp402816b | J. Phys. Chem. C 2013, 117, 13276−13282

HOMO−LUMO gap of **A2** (1.22 eV), so the HOMO−LUMO gap of **A1** should be about 1.03 eV according to our theoretical calculation. We guess that the reasons for the big difference between the theoretical and experimental HOMO−LUMO gaps may be the following: (1) the PBE functional has a deficiency in predicting accurate optical absorption; (2) for some systems, there is a difference between the theoretical HOMO−LUMO gap and the optical gap constitutionally; and (3) the wavelength range (300−750 nm) of optical absorption spectra measured by Wan et al. may be improper. The longer wavelength (>750 nm) should also be scanned in the optical absorption spectra. Coincidently, the experimental value (2.24 eV) is very close to the band edge (2.16 eV) of the second major absorption peak of the simulated UV−vis absorption spectra (Figure 6b), which is not exactly the HOMO−LUMO gap. Certainly, the real reason needs to be further verified by the experimental method. We expect that some new experiments or more accurate theoretical calculations will be carried out to solve the problems of the disagreement between the theoretical and experimental results.

4. CONCLUSIONS

In summary, we have analyzed the structural stability and electronic properties of a newly crystallized cluster $[Au_{20}(PPhpy_2)_{10}Cl_4]Cl_2$ by using DFT. The computed HOMO−LUMO gap of the Au_{20} nanocluster protected by hemilabile phosphines is about 1.03 eV, in agreement with the band edge of simulated UV−vis absorption spectra, but not in agreement with the experimental HOMO−LUMO gap. Certainly, the further determination of the HOMO−LUMO gap still needs to rely on the experimental method or more accurate theoretical calculation. According to MO diagrams and bonding frameworks, the $Au_{20}^{(+6)}$ core is an analogue of F_2 molecule based on the SVB model. MO and chemical bonding analyses reveal that the 20c−14e $Au_{20}^{(+6)}$ core can be taken as a superatomic molecule bonded by two 11c−7e superatoms, where the two 11c superatoms share two Au atoms and two electrons to meet the 8-electron closed shell for each. The electronic shell closure enhances the stability of the Au_{20} core, besides the PN bridges. Therefore, both geometrical and electronic shell closure are responsible for the magic stability of ligand-protected Au clusters. We believe that our work on detailed theoretical analyses of electronic structure will be helpful to understand $[Au_{20}(PPhpy_2)_{10}Cl_4]Cl_2$ cluster deeply. Particularly, the arrangement of the Au_{20} core structure suggests that incomplete icosahedral motifs may be considered in making prediction of the structures of Au clusters, and the superatomic molecule model may be also found in some other ligand-protected Au clusters.

■ ASSOCIATED CONTENT

Supporting Information

XYZ coordinates of **A1** and **A2**. This material is available free of charge via the Internet at http://pubs.acs.org.

■ AUTHOR INFORMATION

Corresponding Author

*E-mail: clj@ustc.edu (L.C.); jlyang@ustc.edu.cn (J.Y.).

Author Contributions

The manuscript was written through contributions of all authors. All authors have given approval to the final version of the manuscript.

Notes

The authors declare no competing financial interest.

■ ACKNOWLEDGMENTS

It is a pleasure to thank Prof. Boldyrev for the AdNDP codes. This work is financed by the National Key Basic Research Program of China (2011CB921404), by the National Natural Science Foundation of China (21121003, 21273008, 21233007, 91021004), by CAS (XDB01020300), and by the 211 Project and the Outstanding Youth Foundation of Anhui University. The calculations were carried out at the High-Performance Computing Center of Anhui University.

■ REFERENCES

(1) Ingram, R. S.; Hostetler, M. J.; Murray, R. W.; Schaaff, T. G.; Khoury, J. T.; Whetten, R. L.; Bigioni, T. P.; Guthrie, D. K.; First, P. N. 28 kDa Alkanethiolate-Protected Au Clusters Give Analogous Solution Electrochemistry and STM Coulomb Staircases. *J. Am. Chem. Soc.* **1997**, *119*, 9279−9280.

(2) Hostetler, M. J.; Wingate, J. E.; Zhong, C.-J.; Harris, J. E.; Vachet, R. W.; Clark, M. R.; Londono, J. D.; Green, S. J.; Stokes, J. J.; Wignall, G. D.; et al. Alkanethiolate Gold Cluster Molecules with Core Diameters from 1.5 to 5.2 nm: Core and Monolayer Properties as a Function of Core Size. *Langmuir* **1998**, *14*, 17−30.

(3) Schmid, G.; Baumle, M.; Geerkens, M.; Heim, I.; Osemann, C.; Sawitowski, T. Current and Future Applications of Nanoclusters. *Chem. Soc. Rev.* **1999**, *28*, 179−185.

(4) Calhorda, M. J.; Crespo, O.; Gimeno, M. C.; Jones, P. G.; Laguna, A.; Lopez-de-Luzuriaga, J. M.; Perez, J. L.; Ramon, M. A.; Veiros, L. F. Synthesis, Structure, Luminescence, and Theoretical Studies of Tetranuclear Gold Clusters with Phosphinocarborane Ligands. *Inorg. Chem.* **2000**, *39*, 4280−4285.

(5) Pei, Y.; Zeng, X. C. Investigating the structural evolution of thiolate protected gold clusters from first-principles. *Nanoscale* **2012**, *4*, 4054−4072.

(6) Schaaff, T. G.; Knight, G.; Shafigullin, M. N.; Borkman, R. F.; Whetten, R. L. Isolation and Selected Properties of a 10.4 kDa Gold:Glutathione Cluster Compound. *J. Phys. Chem. B* **1998**, *102*, 10643−10646.

(7) Schaaff, T. G.; Whetten, R. L. Controlled Etching of Au:SR Cluster Compounds. *J. Phys. Chem. B* **1999**, *103*, 9394−9396.

(8) Schaaff, T. G.; Shafigullin, M. N.; Khoury, J. T.; Vezmar, I.; Whetten, R. L. Properties of a Ubiquitous 29 kDa Au:SR Cluster Compound. *J. Phys. Chem. B* **2001**, *105*, 8785−8796.

(9) Daniel, M.-C.; Astruc, D. Gold Nanoparticles: Assembly, Supramolecular Chemistry, Quantum-Size-Related Properties, and Applications toward Biology, Catalysis, and Nanotechnology. *Chem. Rev.* **2003**, *104*, 293−346.

(10) Donkers, R. L.; Lee, D.; Murray, R. W. Synthesis and Isolation of the Molecule-like Cluster $Au_{38}(PhCH_2CH_2S)_{24}$. *Langmuir* **2004**, *20*, 1945−1952.

(11) Negishi, Y.; Takasugi, Y.; Sato, S.; Yao, H.; Kimura, K.; Tsukuda, T. Magic-Numbered Aun Clusters Protected by Glutathione Monolayers (n = 18, 21, 25, 28, 32, 39): Isolation and Spectroscopic Characterization. *J. Am. Chem. Soc.* **2004**, *126*, 6518−6519.

(12) Ackerson, C. J.; Jadzinsky, P. D.; Kornberg, R. D. Thiolate Ligands for Synthesis of Water-Soluble Gold Clusters. *J. Am. Chem. Soc.* **2005**, *127*, 6550−6551.

(13) Shichibu, Y.; Negishi, Y.; Tsukuda, T.; Teranishi, T. Large-Scale Synthesis of Thiolated Au_{25} Clusters via Ligand Exchange Reactions of Phosphine-Stabilized Au_{11} Clusters. *J. Am. Chem. Soc.* **2005**, *127*, 13464−13465.

(14) Toikkanen, O.; Ruiz, V.; Ronnholm, G.; Kalkkinen, N.; Liljeroth, P.; Quinn, B. M. Synthesis and Stability of Monolayer-Protected Au_{38} Clusters. *J. Am. Chem. Soc.* **2008**, *130*, 11049−11055.

(15) Qian, H.; Jin, R. Synthesis and Electrospray Mass Spectrometry Determination of Thiolate-Protected $Au_{55}(SR)_{31}$ Nanoclusters. *Chem. Commun.* **2011**, *47*, 11462−11464.
(16) Iwasa, T.; Nobusada, K. Theoretical Investigation of Optimized Structures of Thiolated Gold Cluster $[Au_{25}(SCH_3)_{18}]^+$. *J. Phys. Chem. C* **2006**, *111*, 45−49.
(17) Negishi, Y.; Chaki, N. K.; Shichibu, Y.; Whetten, R. L.; Tsukuda, T. Origin of Magic Stability of Thiolated Gold Clusters: A Case Study on $Au_{25}(SC_6H_{13})_{18}$. *J. Am. Chem. Soc.* **2007**, *129*, 11322−11323.
(18) Aikens, C. M. Origin of Discrete Optical Absorption Spectra of $M_{25}(SH)_{18}^-$ Nanoparticles (M = Au, Ag). *J. Phys. Chem. C* **2008**, *112*, 19797−19800.
(19) Akola, J.; Walter, M.; Whetten, R. L.; Hakkinen, H.; Gronbeck, H. On the Structure of Thiolate-Protected Au_{25}. *J. Am. Chem. Soc.* **2008**, *130*, 3756−3757.
(20) Dass, A.; Stevenson, A.; Dubay, G. R.; Tracy, J. B.; Murray, R. W. Nanoparticle MALDI-TOF Mass Spectrometry without Fragmentation: $Au_{25}(SCH_2CH_2Ph)_{18}$ and Mixed Monolayer $Au_{25}(SCH_2CH_2Ph)_{18-x}(L)_x$. *J. Am. Chem. Soc.* **2008**, *130*, 5940−5946.
(21) Zhu, M.; Eckenhoff, W. T.; Pintauer, T.; Jin, R. Conversion of Anionic $[Au_{25}(SCH_2CH_2Ph)_{18}]^-$ Cluster to Charge Neutral Cluster via Air Oxidation. *J. Phys. Chem. C* **2008**, *112*, 14221−14224.
(22) Dharmaratne, A. C.; Krick, T.; Dass, A. Nanocluster Size Evolution Studied by Mass Spectrometry in Room Temperature $Au_{25}(SR)_{18}$ Synthesis. *J. Am. Chem. Soc.* **2009**, *131*, 13604−13605.
(23) Jiang, D.-e.; Dai, S. From Superatomic $Au25(SR)_{18}^-$ to Superatomic $M@Au_{24}(SR)_{18}^q$ Core−Shell Clusters. *Inorg. Chem.* **2009**, *48*, 2720−2722.
(24) Wu, Z.; Gayathri, C.; Gil, R. R.; Jin, R. Probing the Structure and Charge State of Glutathione-Capped $Au_{25}(SG)_{18}$ Clusters by NMR and Mass Spectrometry. *J. Am. Chem. Soc.* **2009**, *131*, 6535−6542.
(25) Angel, L. A.; Majors, L. T.; Dharmaratne, A. C.; Dass, A. Ion Mobility Mass Spectrometry of $Au_{25}(SCH_2CH_2Ph)_{18}$ Nanoclusters. *ACS Nano* **2010**, *4*, 4691−4700.
(26) Jupally, V. R.; Kota, R.; Dornshuld, E. V.; Mattern, D. L.; Tschumper, G. S.; Jiang, D.-e.; Dass, A. Interstaple Dithiol Cross-Linking in $Au_{25}(SR)_{18}$ Nanomolecules: A Combined Mass Spectrometric and Computational Study. *J. Am. Chem. Soc.* **2011**, *133*, 20258−20266.
(27) MacDonald, M. A.; Chevrier, D. M.; Zhang, P.; Qian, H.; Jin, R. The Structure and Bonding of $Au_{25}(SR)_{18}$ Nanoclusters from EXAFS: The Interplay of Metallic and Molecular Behavior. *J. Phys. Chem. C* **2011**, *115*, 15282−15287.
(28) Zhu, M.; Chan, G.; Qian, H.; Jin, R. Unexpected Reactivity of $Au_{25}(SCH_2CH_2Ph)_{18}$ Nanoclusters with Salts. *Nanoscale* **2011**, *3*, 1703−1707.
(29) Parker, J. F.; Fields-Zinna, C. A.; Murray, R. W. The Story of a Monodisperse Gold Nanoparticle: $Au_{25}L_{18}$. *Acc. Chem. Res.* **2010**, *43*, 1289−1296.
(30) Häkkinen, H.; Barnett, R. N.; Landman, U. Electronic Structure of Passivated $Au_{38}(SCH_3)_{24}$ Nanocrystal. *Phys. Rev. Lett.* **1999**, *82*, 3264−3267.
(31) Wang, W.; Murray, R. W. Reaction of Triphenylphosphine with Phenylethanethiolate-Protected Au_{38} Nanoparticles. *Langmuir* **2005**, *21*, 7015−7022.
(32) Jiang, D.-e.; Luo, W.; Tiago, M. L.; Dai, S. In Search of a Structural Model for a Thiolate-protected Au_{38} Cluster. *J. Phys. Chem. C* **2008**, *112*, 13905−13910.
(33) Qian, H.; Zhu, Y.; Jin, R. Size-Focusing Synthesis, Optical and Electrochemical Properties of Monodisperse $Au_{38}(SC_2H_4Ph)_{24}$ Nanoclusters. *ACS Nano* **2009**, *3*, 3795−3803.
(34) Lopez-Acevedo, O.; Tsunoyama, H.; Tsukuda, T.; Hakkinen, H.; Aikens, C. M. Chirality and Electronic Structure of the Thiolate-Protected Au_{38} Nanocluster. *J. Am. Chem. Soc.* **2010**, *132*, 8210−8218.
(35) Qian, H.; Eckenhoff, W. T.; Zhu, Y.; Pintauer, T.; Jin, R. Total Structure Determination of Thiolate-Protected Au_{38} Nanoparticles. *J. Am. Chem. Soc.* **2010**, *132*, 8280−8281.
(36) Knoppe, S.; Boudon, J.; Dolamic, I.; Dass, A.; Burgi, T. Size Exclusion Chromatography for Semipreparative Scale Separation of $Au_{38}(SR)_{24}$ and $Au_{40}(SR)_{24}$ and Larger Clusters. *Anal. Chem.* **2011**, *83*, 5056−5061.
(37) MacDonald, M. A.; Zhang, P.; Chen, N.; Qian, H.; Jin, R. Solution-Phase Structure and Bonding of $Au_{38}(SR)_{24}$ Nanoclusters from X-ray Absorption Spectroscopy. *J. Phys. Chem. C* **2011**, *115*, 65−69.
(38) Cheng, L.; Ren, C.; Zhang, X.; Yang, J. New Insight into Electronic Shell of $Au_{38}(SR)_{24}$: A Superatomic Molecule. *Nanoscale* **2013**, *5*, 1475−1478.
(39) Knoppe, S.; Dolamic, I.; Dass, A.; Burgi, T. Separation of Enantiomers and CD Spectra of $Au_{40}(SCH_2CH_2Ph)_{24}$: Spectroscopic Evidence for Intrinsic Chirality. *Angew. Chem., Int. Ed.* **2012**, *51*, 7589−7591.
(40) Malola, S. A.; Lehtovaara, L.; Knoppe, S.; Hu, K. J.; Palmer, R. E.; Burgi, T.; Hakkinen, H. J. $Au_{40}(SR)_{24}$ Cluster as a Chiral Dimer of 8-Electron Superatoms: Structure and Optical Properties. *J. Am. Chem. Soc.* **2012**, *134*, 19560−19563.
(41) Gao, Y.; Shao, N.; Zeng, X. C. Ab Initio Study of Thiolate-Protected Au_{102} Nanocluster. *ACS Nano* **2008**, *2*, 1497−1503.
(42) Li, Y.; Galli, G.; Gygi, F. Electronic Structure of Thiolate-Covered Gold Nanoparticles: $Au_{102}(MBA)_{44}$. *ACS Nano* **2008**, *2*, 1896−1902.
(43) Qian, H.; Zhu, Y.; Jin, R. Isolation of Ubiquitous $Au_{40}(SR)_{24}$ Clusters from the 8 kDa Gold Clusters. *J. Am. Chem. Soc.* **2010**, *132*, 4583−4585.
(44) Schnockel, H.; Schnepf, A.; Whetten, R. L.; Schenk, C.; Henke, P. A Chemical View of the Giant $Au_{102}(SR)_{44}$ (SR = *p*-Mercaptobenzoic Acid) Cluster: Metalloid Aluminum and Gallium Clusters as Path Making Examples of This Novel Type Open Our Eyes for Structure and Bonding of Metalloid $Au_n(SR)_m$ ($n > m$) Clusters. *Z. Anorg. Allg. Chem.* **2011**, *637*, 15−23.
(45) Walter, M.; Akola, J.; Lopez-Acevedo, O.; Jadzinsky, P. D.; Calero, G.; Ackerson, C. J.; Whetten, R. L.; Gronbeck, H.; Hakkinen, H. A Unified View of Ligand-Protected Gold Clusters as Superatom Complexes. *Proc. Natl. Acad. Sci. U. S. A.* **2008**, *105*, 9157−9162.
(46) Lopez-Acevedo, O.; Akola, J.; Whetten, R. L.; Gronbeck, H.; Hakkinen, H. Structure and Bonding in the Ubiquitous Icosahedral Metallic Gold Cluster $Au_{144}(SR)_{60}$. *J. Phys. Chem. C* **2009**, *113*, 5035−5038.
(47) Qian, H.; Jin, R. Controlling Nanoparticles with Atomic Precision: The Case of $Au_{144}(SCH_2CH_2Ph)_{60}$. *Nano Lett.* **2009**, *9*, 4083−4087.
(48) Koivisto, J.; Malola, S.; Kumara, C.; Dass, A.; Hakkinen, H.; Pettersson, M. Experimental and Theoretical Determination of the Optical Gap of the $Au_{144}(SC_2H_4Ph)_{60}$ Cluster and the $(Au/Ag)_{144}(SC_2H_4Ph)_{60}$ Nanoalloys. *J. Phys. Chem. Lett.* **2012**, *3*, 3076−3080.
(49) Heaven, M. W.; Dass, A.; White, P. S.; Holt, K. M.; Murray, R. W. Crystal Structure of the Gold Nanoparticle $[N(C_8H_{17})_4][Au_{25}(SCH_2CH_2Ph)_{18}]$. *J. Am. Chem. Soc.* **2008**, *130*, 3754−3755.
(50) Zhu, M.; Aikens, C. M.; Hollander, F. J.; Schatz, G. C.; Jin, R. Correlating the Crystal Structure of a Thiol-Protected Au_{25} Cluster and Optical Properties. *J. Am. Chem. Soc.* **2008**, *130*, 5883−5885.
(51) Zeng, C.; Qian, H.; Li, T.; Li, G.; Rosi, N. L.; Yoon, B.; Barnett, R. N.; Whetten, R. L.; Landman, U.; Jin, R. Total Structure and Electronic Properties of the Gold Nanocrystal $Au_{36}(SR)_{24}$. *Angew. Chem., Int. Ed.* **2012**, *124*, 13291−13295.
(52) Jadzinsky, P. D.; Calero, G.; Ackerson, C. J.; Bushnell, D. A.; Kornberg, R. D. Structure of a Thiol Monolayer-Protected Gold Nanoparticle at 1.1 Å Resolution. *Science* **2007**, *318*, 430−433.
(53) Pei, Y.; Gao, Y.; Zeng, X. C. Structural Prediction of Thiolate-Protected Au_{38}: A Face-Fused Bi-icosahedral Au Core. *J. Am. Chem. Soc.* **2008**, *130*, 7830−7832.
(54) Lopez-Acevedo, O.; Tsunoyama, H.; Tsukuda, T.; Aikens, C. M. Chirality and Electronic Structure of the Thiolate-Protected Au_{38} Nanocluster. *J. Am. Chem. Soc.* **2010**, *132*, 8210−8218.

(55) Zhang, D.; Dou, J.; Li, D.; Wang, D. Synthesis, Characterization and Luminescence of the Tetranuclear Gold Cluster: $[Au_4\{7,8\text{-}(PPh_2)_2\text{-}7,8\text{-}C_2B_9H_{10}\}_2(PPh_3)_2]$. *J. Coord. Chem.* **2007**, *60*, 825−831.
(56) Jones, P. G. X-ray Structural Investigations of Gold Compounds. *Gold Bull.* **1983**, *16*, 114−124.
(57) Van der Velden, J.; Bour, J.; Bosman, W.; Noordik, J. Reactions of Cationic Gold Clusters with Lewis Bases. Preparation and X-ray Structure Investigation of $[Au_8(PPh_3)_7](NO_3)_2.2CH_2Cl_2$ and $Au_6(PPh_3)_4[Co(CO)_4]_2$. *Inorg. Chem.* **1983**, *22*, 1913−1918.
(58) Briant, C. E.; Hall, K. P.; Mingos, D. M. P. Structural Characterisation of Two Crystalline Modifications of $[Au_9\{P(C_6H_4OMe\text{-}p)_3\}_8](NO_3)_3$: The First Example of Skeletal Isomerism in Metal Cluster Chemistry. *J. Chem. Soc., Chem. Commun.* **1984**, 290−291.
(59) Laguna, A.; Laguna, M.; Gimeno, M. C.; Jones, P. G. Synthesis and X-ray Characterization of the Neutral Organometallic Gold Cluster $[Au_{10}(C_6F_5)_4(PPh_3)_5]$. *Organometallics* **1992**, *11*, 2759−2760.
(60) Copley, R. C. B.; Mingos, D. M. P. The Novel Structure of the $[Au_{11}(PMePh_2)_{10}]^{3+}$ Cation: Crystal Structures of $[Au_{11}(PMePh_2)_{10}][C_2B_9H_{12}]_3.4thf$ and $[Au_{11}(PMePh_2)_{10}][C_2B_9H_{12}]_3$ (thf = tetrahydrofuran). *J. Chem. Soc., Dalton Trans.* **1996**, 479−489.
(61) Menard, L. D.; Xu, H.; Gao, S. P.; Twesten, R. D.; Harper, A. S.; Song, Y.; Wang, G.; Douglas, A. D.; Yang, J. C.; Frenkel, A. I. Metal Core Bonding Motifs of Monodisperse Icosahedral Au_{13} and Larger Au Monolayer-Protected Clusters As Revealed by X-ray Absorption Spectroscopy and Transmission Electron Microscopy. *J. Phys. Chem. B* **2006**, *110*, 14564−14573.
(62) Li, J.; Wang, S. G. Phosphane-Stabilized Gold Clusters: Investigation of the Stability of $[Au_{13}(PMe_2Ph)_{10}Cl_2]^{3+}$. *J. Mol. Model.* **2010**, *16*, 505−512.
(63) Das, A.; Li, T.; Nobusada, K.; Zeng, Q.; Rosi, N. L.; Jin, R. Total Structure and Optical Properties of a Phosphine/Thiolate-Protected Au_{24} Nanocluster. *J. Am. Chem. Soc.* **2012**, *134*, 20286−20289.
(64) Teo, B. K.; Shi, X.; Zhang, H. Pure Gold Cluster of 1:9:9:1:9:9:1 Layered Structure: A Novel 39-Metal-Atom Cluster $[(Ph_3P)_{14}Au_{39}Cl_6]Cl_2$ with an Interstitial Gold Atom in a Hexagonal Antiprismatic Cage. *J. Am. Chem. Soc.* **1992**, *114*, 2743−2745.
(65) Schmid, G.; Liu, Y. P.; Schumann, M.; Raschke, T.; Radehaus, C. Quasi One-Dimensional Arrangements of $Au_{55}(PPh_3)_{12}Cl_6$ Clusters and Their Electrical Properties at Room Temperature. *Nano Lett.* **2001**, *1*, 405−407.
(66) Schmid, G. The Relevance of Shape and Size of Au_{55} Clusters. *Chem. Soc. Rev.* **2008**, *37*, 1909−1930.
(67) Pei, Y.; Shao, N.; Gao, Y.; Zeng, X. C. Investigating Active Site of Gold Nanoparticle $Au_{55}(PPh_3)_{12}Cl_6$ in Selective Oxidation. *ACS Nano* **2010**, *4*, 2009−2020.
(68) Carr, J. A.; Wang, H.; Abraham, A.; Gullion, T.; Lewis, J. P. L-Cysteine Interaction with Au_{55} Nanoparticle. *J. Phys. Chem. C* **2012**, *116*, 25816−25823.
(69) Wan, X. K.; Lin, Z. W.; Wang, Q. M. Au_{20} Nanocluster Protected by Hemilabile Phosphines. *J. Am. Chem. Soc.* **2012**, *134*, 14750−14752.
(70) Zhu, M.; Lanni, E.; Garg, N.; Bier, M. E.; Jin, R. Kinetically Controlled, High-Yield Synthesis of Au_{25} Clusters. *J. Am. Chem. Soc.* **2008**, *130*, 1138−1139.
(71) Tsunoyama, H.; Nickut, P.; Negishi, Y.; Al-Shamery, K.; Matsumoto, Y.; Tsukuda, T. Formation of Alkanethiolate-Protected Gold Clusters with Unprecedented Core Sizes in the Thiolation of Polymer-Stabilized Gold Clusters. *J. Phys. Chem. C* **2007**, *111*, 4153−4158.
(72) Qian, H.; Zhu, M.; Andersen, U. N.; Jin, R. Facile, Large-Scale Synthesis of Dodecanethiol-Stabilized Au_{38} Clusters. *J. Phys. Chem. A* **2009**, *113*, 4281−4284.
(73) Perdew, J. P.; Burke, K.; Ernzerhof, M. Generalized gradient approximation made simple. *Phys. Rev. Lett.* **1996**, *77*, 3865−3868.
(74) Tlahuice, A.; Garzon, I. L. On the Structure of the $Au_{18}(SR)_{14}$ Cluster. *Phys. Chem. Chem. Phys.* **2012**, *14*, 3737−3740.
(75) Aikens, C. M. Geometric and Electronic Structure of $Au_{25}(SPhX)_{18}^-$ (X = H, F, Cl, Br, CH_3, and OCH_3). *J. Phys. Chem. Lett.* **2010**, *1*, 2594−2599.
(76) Frisch, M. J.; Trucks, G. W.; Schlegel, H. B.; Scuseria, G. E.; Robb, M. A.; Cheeseman, J. R.; Scalmani, G.; Barone, V.; Mennucci, B.; Petersson, G. A.; et al. *Gaussian 09, revision B.01*; Gaussian, Inc., Wallingford CT, 2009.
(77) Zubarev, D. Y.; Boldyrev, A. I. Comprehensive Analysis of Chemical Bonding in Boron Clusters. *J. Comput. Chem.* **2007**, *28*, 251−268.
(78) Zubarev, D. Y.; Boldyrev, A. I. Developing Paradigms of Chemical Bonding: Adaptive Natural Density Partitioning. *Phys. Chem. Chem. Phys.* **2008**, *10*, 5207−5217.
(79) Zubarev, D. Y.; Boldyrev, A. I. Revealing Intuitively Assessable Chemical Bonding Patterns in Organic Aromatic Molecules via Adaptive Natural Density Partitioning. *J. Org. Chem.* **2008**, *73*, 9251−9258.
(80) Sergeeva, A. P.; Averkiev, B. B.; Zhai, H. J.; Boldyrev, A. I.; Wang, L. S. All-Boron Analogues of Aromatic Hydrocarbons: B_{17}^- and B_{18}^-. *J. Chem. Phys.* **2011**, *134*, 224304.
(81) Cheng, L. J. B_{14}: An All-Boron Fullerene. *J. Chem. Phys.* **2012**, *136*, 104301.
(82) Yuan, Y.; Cheng, L. B_{14}^{2+}: A Magic Number Double-Ring Cluster. *J. Chem. Phys.* **2012**, *137*, 044308.
(83) Zubarev, D. Y.; Boldyrev, A. I. Deciphering chemical bonding in golden cages. *J. Phys. Chem. A* **2008**, *113*, 866−868.
(84) Cheng, L.; Yang, J. New Insight into Electronic Shells of Metal Clusters: Analogues of Simple Molecules. *J. Chem. Phys.* **2013**, *138*, 141101.
(85) Burgess, R.; Keast, V. TDDFT Study of the Optical Absorption Spectra of Bare and Coated Au_{55} and Au_{69} Clusters. *J. Phys. Chem. C* **2011**, *115*, 21016−21021.
(86) Li, J.; Li, X.; Zhai, H.-J.; Wang, L.-S. Au_{20}: A Tetrahedral Cluster. *Science* **2003**, *299*, 864−867.